(ces domaines ne présentent que des déformations d'allongement) et, pour les domaines '*a*' où

$$d_{14}=d_{15}, \text{ à}$$
$$x_4=d_{15}E_2=d_{15}E \qquad (3)$$

(ces domaines ne présentent que des déformations de cisaillement).

Les observations faites s'expliquent par les relations (1), (2) et (3). Excepté au voisinage des domaines '*a*', les déformations du cristal '*c*' consistent essentiellement en un allongement de la maille conformément aux équations (2).

Par contre les domaines '*a*' sont soumis à un cisaillement mais l'équation (3) n'est pas applicable, ces domaines petits n'étant pas libres de contraintes. Les mouvements de rotation observés sont en relation avec cet effet dont l'influence s'étend aux domaines '*c*' contigus.

Compte tenu des difficultés d'analyse des déformations d'une structure polydomaine, le seul résultat quantitatif rigoureux concerne le coefficient d_{33}. C'est ainsi que les rotations observées pour les domaines '*a*' sont supérieures à la rotation qui serait dûe à un simple cisaillement, compte tenu de la valeur de d_{15} ($11{,}76 \cdot 10^{-6}$ C.G.S.) donnée par Berlincourt & Jaffe (1958).

La déformation piézoélectrique d'allongement enregistrée pour le domaine '*c*' loin des parois est constante quelque soit la rotation subie par les plans au point considéré. La valeur numérique du coèfficient piézoélectrique d_{33} obtenu est $4{,}6 \cdot 10^{-6}$ C.G.S.

La valeur donnée par Berlincourt & Jaffe est $2{,}57 \cdot 10^{-6}$ C.G.S., tandis que la valeur de Caspari & Merz (1950) est $3{,}96 \cdot 10^{-6}$ C.G.S., mais il s'agissait de mesures macroscopiques qui sont moins significatives si l'on a pas affaire à un cristal parfaitement monodomaine.

Pour la région 4, les équations (2) donneraient les valeurs plus élevées $7{,}5 \cdot 10^{-6}$ et $9 \cdot 10^{-6}$ C.G.S. En fait ces équations ne sont plus valables en raison des contraintes.

Conclusion

On a voulu montrer le caractère complexe du comportement structural des cristaux de titanate de baryum avec et sans champ électrique appliqué; on a pu mettre en évidence des rotations d'axes parallèles aux frontières des domaines sous l'action du champ, des déformations de la maille variable d'un point à l'autre. Avec les modifications apportées à la méthode de Lambot–Vassamillet la carte des variations spaciales des distances réticulaires et des désorientations peut être obtenue sans ambiguité et avec une bonne précision, en utilisant des temps de pose très courts et avec des réglages aisés.

Références

ANLIKER, M., BRUGGER, H. R. & KANZIG, W. (1954). *Helv. Phys. Acta*, **27**, 99.

BERLINCOURT, D. & JAFFE, H. (1958). *Phys. Rev.* **80**, 1082.

BOUSQUET, C., LAMBERT, M., QUITTET, A. M. & GUINIER, A. (1963). *Acta Cryst.* **16**, 989.

CASPARI, M. E. & MERZ, W. J. (1950). *Phys. Rev.* **111**, 143.

LAMBERT, M., QUITTET, A. M., TAUPIN, C. & GUINIER, A. (1964). *J. Phys. Radium*, **25**, 345.

LAMBOT, H., VASSAMILLET, L. & DEJACE, J. (1953). *Acta Metallurg.* **1**, 711.

REMEIKA, J. P. (1954). *J. Amer. Chem. Soc.* **76**, 940.

Acta Cryst. (1967). **23**, 357

The Resolution Function in Neutron Diffractometry
I. The Resolution Function of a Neutron Diffractometer and its Application to Phonon Measurements*

BY M. J. COOPER† AND R. NATHANS
Brookhaven National Laboratory, Upton, New York, U.S.A.

(*Received* 31 *October* 1966)

The general features of the resolution function of a crystal diffractometer and its experimental determination are considered. An analytic expression is derived for its form for a three-crystal diffractometer assuming Gaussian mosaic and collimation functions. Under these conditions the loci of constant probability are shown to be ellipsoids and the application of the resolution function to neutron measurements is discussed with particular reference to inelastic phonon measurements. Experimental evidence is presented in support of these considerations.

Introduction

The resolution of neutron diffractometers has been considered by a number of authors because of two substantially different effects which it may have on the results of neutron scattering experiments.

On the one hand focusing effects may result in increasing both the maximum intensity and the sharpness of diffraction peaks, as has been discussed by Caglioti and his coworkers (Caglioti, Paoletti & Ricci, 1958, 1960; Caglioti & Ricci, 1962; Caglioti, 1964; Caglioti & Tocchetti, 1964, 1965), Shull (1960) and Willis (1960)

* Work performed under the auspices of the U.S. Atomic Energy Commission.

† Present address: Atomic Energy Research Establishment, Harwell, Berks, England.

for the case of Bragg reflections and by Collins (1963) and others for the case of inelastic phonon scattering. The focusing conditions depend on the collimation and on the mosaic spread of the monochromator and analyzer crystals and these authors have examined in detail the best choice of the various adjustable parameters to utilize the focusing effects always present in crystal diffractometers.

On the other hand it may be the detailed form of the scattering cross section which is of interest, in which case the parameters should be chosen so that this can be determined most accurately. Under these conditions, some types of focusing may be a severe disadvantage. A detailed consideration of the resolution function is then essential for a satisfactory analysis of the experimental results, both in the investigation of some types of diffuse scattering, for example critical magnetic scattering, and in the detailed study of peak shapes and widths, for example broadening of inelastic scattering peaks due to the finite life-times of phonons and magnons.

It is our purpose in the present work to consider under what conditions it is possible to make accurate resolution corrections to the observed data and to present supporting experimental evidence. In the present paper we shall discuss the resolution function in general terms and then consider in detail its determination for a three-crystal diffractometer and its application to phonon measurements. In a later paper we shall then consider the resolution function for a two-crystal diffractometer and its application to the measurement of both diffuse scattering and Bragg reflections.

Definition of the resolution function

The layout of a typical three-crystal diffractometer is illustrated in Fig. 1; in a two-crystal diffractometer the analyzer is omitted and the detector is mounted to receive directly the neutrons scattered by the sample at the desired angle. $2\theta_M, 2\theta_S, 2\theta_A$ are the scattering angles of the monochromator, sample, and analyzer respectively.

The resolution of the diffractometer is best considered in reciprocal space. We associate a scattering process in which the neutron loses an energy $\hbar\omega$ for a change in momentum of $\hbar\mathbf{Q}$ with a particular point in $\omega, \mathbf{Q}$ space. The settings of $2\theta_M$, $2\theta_S$ and $2\theta_A$ define the point in $\omega, \mathbf{Q}$ space for which the probability of detection is highest, according to the relations:

$$k_I = \frac{\pi}{d_M \sin\theta_M} \qquad k_F = \frac{\pi}{d_A \sin\theta_A} \tag{1}$$

$$\mathbf{Q}_0 = \mathbf{k}_F - \mathbf{k}_I \tag{2}$$

$$\hbar\omega_0 = \frac{\hbar^2}{2m}(k_I^2 - k_F^2) \tag{3}$$

where d_M and d_A are the d spacings of the monochromator and analyzer respectively and the angle between $\mathbf{k}_F$ and $\mathbf{k}_I$ is $2\theta_S$.

However, the presence of finite collimation and finite mosaic spread in the monochromator and analyzer allow less probable neutrons to be detected at the same settings. The resolution function of the instrument is the probability of detection of neutrons as a function of $\Delta\omega$ and $\Delta\mathbf{Q}$ when the instrument has been set to measure a scattering process corresponding to the point $\omega_0, \mathbf{Q}_0$.

Method of determination

In order to calculate the resolution function we assume that the transmission function of a Soller slit collimator and the mosaic spreads of the monochromator and analyzer are Gaussian distributions. This assumption allows us to calculate explicitly an analytic form for the resolution function at any point in $\omega, \mathbf{Q}$ space for any set of values for the instrumental parameters.

Although the mosaic spreads of the crystals and the divergence angles of the collimators can be determined independently, the values so obtained may not be the effective values for the instrument as a whole. The following procedure may therefore be adopted for determining the effective values indirectly. By scanning a number of Bragg reflections from a perfect crystal sample the resolution function in $\omega, \mathbf{Q}$ space for these particular configurations can be determined and the effective instrumental parameters calculated.

The collimating properties of Soller slit systems have been discussed by Sailor, Foote, Landon & Wood (1956), who point out that although the angular transmission function for these should be triangular, in practice imperfections and critical reflection lead to a function which is more nearly Gaussian in shape. These authors were concerned with fine collimation systems

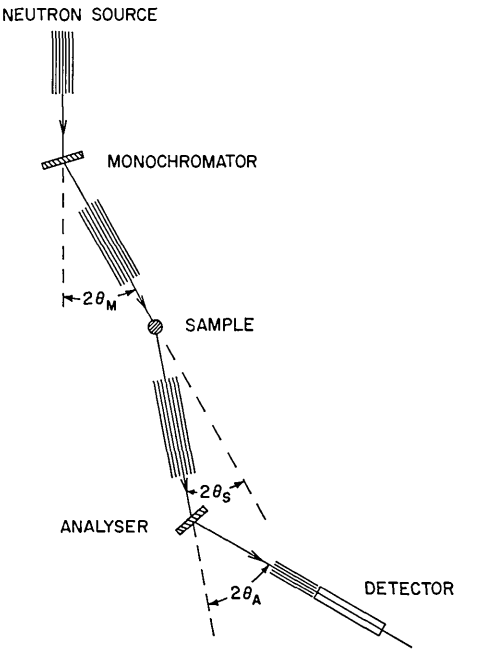

Fig. 1. Layout of a typical three-crystal diffractometer.

(< 10′). We have been able to confirm that the larger divergence systems (10–40′) used in conventional diffractometers can have angular transmission functions which are essentially Gaussian in form over an appreciable angle. However, we may note that Shull (1960) has carried out resolution calculations for a triangular function and finds the results to be very closely the same as for a Gaussian function.

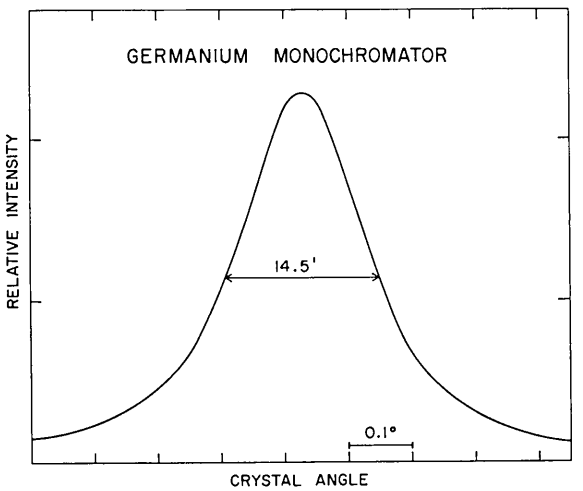

Fig. 2. Observed rocking curve for the 220 reflection of a distorted germanium crystal.

While the Gaussian form for the mosaic spread of ideally imperfect crystals is usually assumed in most extinction calculations, the large metal single crystals required for the monochromator and analyzer are usually found to have a lineage structure which varies from point to point on the crystal. However, the procedure adopted by Barrett, Mueller & Heaton (1963) to distort relatively perfect germanium crystals* has been found to produce crystals with Gaussian shaped rocking curves of about 15–30′ full width at half height, as shown in Fig. 2. These crystals are used in transmission geometry which, combined with their mosaic uniformity, leads to highly homogeneous monochromatized neutron beams.

Derivation of the resolution function

Fig. 3 shows a vector diagram in reciprocal space. $\mathbf{k}_I(PO)$ is the wave vector of the most probable incident neutron from the monochromator; $\mathbf{k}_F(PQ)$ is the wave vector of this neutron after scattering through an angle $2\theta_S$ and an energy transfer for optimum acceptance by the analyzer. $\mathbf{k}_i$ and $\mathbf{k}_f$ are wave vectors corresponding to any scattering process in the sample and we shall define $\Delta\mathbf{k}_i=\mathbf{k}_i-\mathbf{k}_I$ and $\Delta\mathbf{k}_f=\mathbf{k}_f-\mathbf{k}_F$. We define

* As adapted in this laboratory by Dr Cox, Mr Hurst, and Mr Merkert.

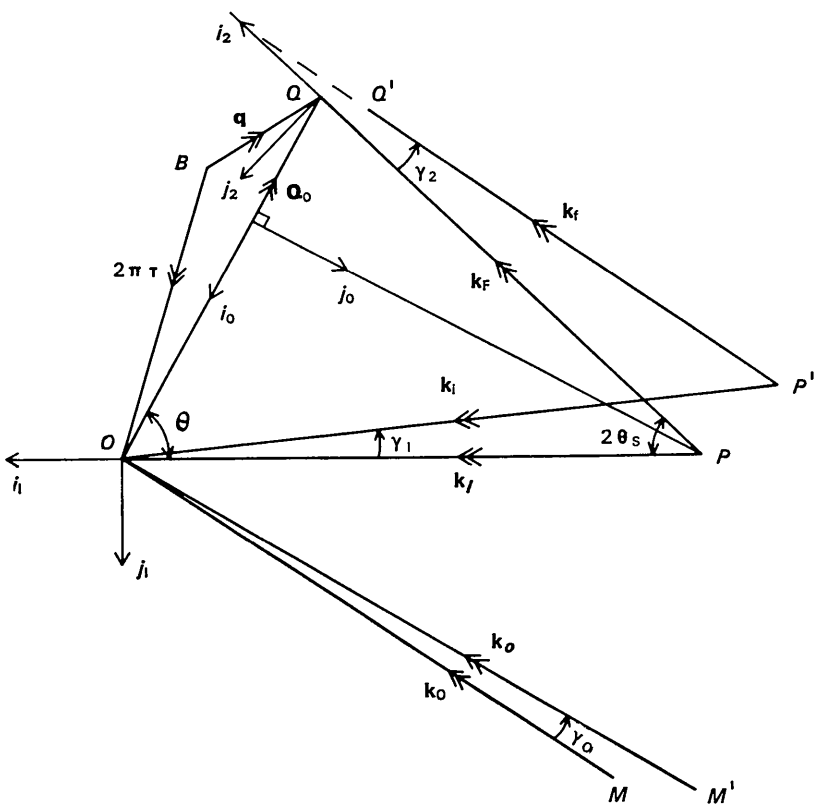

Fig. 3. Vector diagram in reciprocal space for a general scattering process.

also the horizontal and vertical divergence angles with respect to the optimum directions to be $\gamma_0,\gamma_1,\gamma_2,\gamma_3$, and $\delta_0,\delta_1,\delta_2,\delta_3$, respectively, where 0, 1, 2, and 3 refer to in-pile, monochromator to sample, sample to analyzer, and analyzer to detector regions respectively and all divergence angles are measured in the same sense (*e.g.* all γ's counterclockwise in Fig. 3).

If there is no correlation between wave number and direction in the neutron beam striking the monochromator then the beam reflected from it will be correlated only with respect to its horizontal divergence. If the monochromator is set to reflect the required wavelength with maximum reflectivity P_M, then assuming a Gaussian mosaic spread defined by η_M (defined as the angle of mis-set of the crystal to give a probability of reflection of $\exp(-\frac{1}{2})$ times the optimum probability) the probability of reflection for a general neutron is:

$$P(\Delta k_i,\gamma_1)=P_M\exp\left\{-\frac{1}{2}\left(\frac{(\Delta k_i/k_I)\tan\theta_M+\gamma_1}{\eta_M}\right)^2\right\}, \tag{4}$$

where θ_M is the Bragg angle of the monochromator for k_I [equation (1)] and we assume that Δk_i is small compared with k_I.

Similarly, the probability of reflection by the analyzer of a general scattered neutron is:

$$P(\Delta k_f,\gamma_2)=P_A\exp\left\{-\frac{1}{2}\left(\frac{(\Delta k_f/k_F)\tan\theta_A-\gamma_2}{\eta_A}\right)^2\right\}, \tag{5}$$

where θ_A is the Bragg angle of the analyzer for k_F [equation (1)], P_A is the optimum reflectivity of the crystal, η_A defines its mosaic spread (analogous to η_M) and we assume that Δk_f is small compared with k_F.

Introducing now the transmission functions of the Soller slit systems, the probability of a neutron being detected is:

$$\begin{aligned}P(\Delta k_i,\Delta k_f,\gamma_1,\gamma_2,\delta_1,\delta_2)&\\ =P_MP_AP_0\exp\Bigg\{-\frac{1}{2}\Bigg[&\left(\frac{(\Delta k_i/k_I)\tan\theta_M+\gamma_1}{\eta_M}\right)^2\\ &+\left(\frac{(\Delta k_f/k_F)\tan\theta_A-\gamma_2}{\eta_A}\right)^2\\ &+\left(\frac{2(\Delta k_i/k_I)\tan\theta_M+\gamma_1}{\alpha_0}\right)^2+\frac{\gamma_1^2}{\alpha_1^2}+\frac{\gamma_2^2}{\alpha_2^2}\\ &+\left(\frac{2(\Delta k_f/k_F)\tan\theta_A-\gamma_2}{\alpha_3}\right)^2+\left(\frac{\delta_1^2}{4\tan^2\theta_M\eta_M'^2+\beta_0^2}\right)\\ &+\frac{\delta_1^2}{\beta_1^2}+\frac{\delta_2^2}{\beta_2^2}+\left(\frac{\delta_2^2}{4\tan^2\theta_A\eta_A'^2+\beta_3^2}\right)\Bigg]\Bigg\},\end{aligned} \tag{6}$$

where $\alpha_0,\alpha_1,\alpha_2,\alpha_3$ and $\beta_0,\beta_1,\beta_2,\beta_3$ are the characteristic horizontal and vertical angles of the collimators defined so that the probability of transmission of a neutron with divergence angle α_0 (for example) is $\exp(-\frac{1}{2})\times P(\alpha_0=0)$. P_0 and the expressions given for the in-pile collimation terms (in α_0,β_0) are derived in Appendix I: the expressions for the detector collimation terms can be derived in the same way. In many instances the in-pile and detector collimations may be sufficiently relaxed for the corresponding terms to be ignored.

This expression for the probability can be separated into two independent terms, a horizontal term $P_H(\Delta k_i,\Delta k_f,\gamma_1,\gamma_2)$ and a vertical term $P_V(\delta_1,\delta_2)$, such that the total probability $P=P_H\times P_V$. The value of the resolution function at a given point in $\omega,\mathbf{Q}$ space is then obtained by integrating the probability over all possible paths $(\mathbf{k}_i,\mathbf{k}_f)$ to that point:

$$R(\omega,\mathbf{Q})=\int P(\omega,\mathbf{Q})\mathbf{dk}_i\mathbf{dk}_f\,. \tag{7}$$

Before integration we transform our variables into $\omega,\mathbf{Q}$ space and hence determine $R(\omega_0+\Delta\omega,\mathbf{Q}_0+\Delta\mathbf{Q})$. The details of this calculation are given in Appendix II, where it is shown that we can write the resolution function in the form:

$$R(\omega_0+\Delta\omega,\mathbf{Q}_0+\Delta\mathbf{Q})=R_0\exp\{-\tfrac{1}{2}\sum_{k=1}^{4}\sum_{l=1}^{4}M_{kl}X_kX_l\}\,, \tag{8}$$

where $X_1=\Delta Q_x, X_2=\Delta Q_y, X_3=\Delta Q_z, X_4=\Delta\omega$ and for convenience X_1 is taken parallel to $\mathbf{Q}_0$ and X_3 is taken to be vertical. R_0 is the optimum value of the resolution function $R(\omega_0,\mathbf{Q}_0)$.

R_0 and M_{kl} are involved functions of $k_I,\omega_0,\mathbf{Q}_0$ and $\eta_M,\eta_A,d_M,d_A,\alpha_0,\alpha_1,\alpha_2,\alpha_3,\beta_0,\beta_1,\beta_2,\beta_3$ but the dependence of the resolution function on $\Delta\omega$ and $\Delta\mathbf{Q}$ is quite simple, being Gaussian for any straight line through $\omega_0\mathbf{Q}_0$. Further, by setting the summation in the exponent in equation (8) equal to p we define the locus of points in $\omega,\mathbf{Q}$ space for which the resolution function has a value $R_0\exp(-p/2)$ which is seen to be an ellipsoid:

$$\sum_{k=1}^{4}\sum_{l=1}^{4}M_{kl}X_kX_l=p\,. \tag{9}$$

It is therefore convenient to visualize the resolution function by considering the 50% (of R_0) probability ellipsoid, for which $p=1{\cdot}386$. We shall refer to this ellipsoid as the resolution ellipsoid and illustrate its form in Fig. 4 for several sets of instrumental parameters.

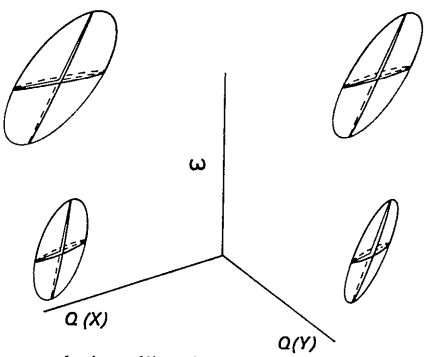

Fig. 4. The resolution ellipsoid for a set of typical instrumental parameters with various values of d_A. Relative scales: 1 Å$^{-1}(Q)\equiv$ 10 Å$^{-2}(\omega)$.

The observed intensity for a given scattering cross section will be:

$$I(\omega_0, \mathbf{Q}_0) = \int R(\omega_0 + \Delta\omega, \mathbf{Q}_0 + \Delta\mathbf{Q}) \cdot \sigma(\omega_0 + \Delta\omega, \mathbf{Q}_0 + \Delta\mathbf{Q}) \Delta\mathbf{Q} \Delta\omega \,. \quad (10)$$

If we have a cross section which is a δ function at a particular point in $\omega, \mathbf{Q}$ space we can measure directly the magnitude of the resolution function at that point. Such a cross section is available in a Bragg reflection from a perfect crystal and we can use this to determine the resolution function in the plane $\omega = 0, \mathbf{Q} = \mathbf{Q}_B = 2\pi\tau$. However, we are not able to move this δ function continuously in $\omega, \mathbf{Q}$ space, and to determine the resolution function for points off this plane we must assume that we can consider the resolution function to be independent of ω_0 and Q_x for small deviations of these from the values 0 and Q_B, an assumption which is in general valid unless Q_0 becomes very small. That is, we assume

$$R(\Delta\omega_0 + \Delta\omega, \mathbf{Q}_B + \Delta\mathbf{Q}_0 + \Delta\mathbf{Q}) = R(\Delta\omega, \mathbf{Q}_B + \Delta\mathbf{Q}) \quad (11)$$

for small $\Delta\omega_0, \Delta\mathbf{Q}_0 (\| \mathbf{Q}_B)$.

Pictorially we are then scanning the resolution function through the Bragg peak instead of scanning the Bragg peak through the resolution function.

The results of such a determination using a perfect single crystal of germanium ($\eta \gtrsim 0{\cdot}1'$) and Gaussian 'distorted' germanium crystals as monochromator and analyzer are illustrated in Fig. 5, which shows sections of the ellipsoid in the $\Delta Q_x, \Delta Q_y$; $\Delta Q_x, \Delta\omega$ and $\Delta Q_y, \Delta\omega$ planes; for convenience we have plotted this in terms of $\Delta E (= \hbar\Delta\omega)$. Fig. 5 shows also a typical ΔQ_z dependence of the resolution function.

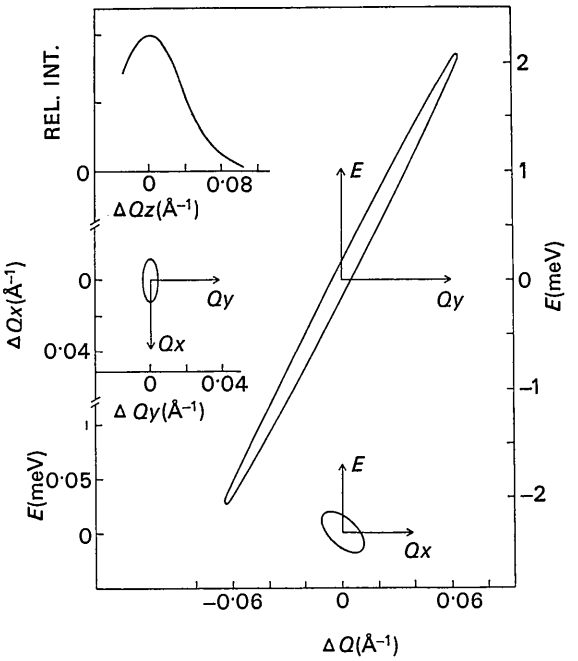

Fig. 5. Sections of an experimentally determined resolution ellipsoid and a typical ΔQ_z dependence of the resolution function.

The experimental resolution function has the form predicted by the analytic expression and we are thus able to compare it directly with that calculated from the instrumental parameters $\eta_M, \eta_A, \alpha_0, \alpha_1, \alpha_2, \alpha_3$. Having confirmed these parameters we can then calculate the resolution function at any point in $\omega, \mathbf{Q}$ space, the dependence on ΔQ_z being independent of position.

Application to phonon measurements

Intensities and line shapes

We see from equation (10) that the intensity observed for a given setting of the diffractometer $(\omega_0, \mathbf{Q}_0)$ is given by the convolution of the scattering cross section with the resolution function centered on $\omega_0, \mathbf{Q}_0$. For phonon scattering we have a surface in $\omega, \mathbf{Q}$ space for which the cross section is finite. We shall call this the dispersion surface and we shall assume that to a first approximation the cross section is constant for that part of the surface over which the resolution function is appreciable. We shall also assume for the moment that the width of the surface is a δ function, that is we shall ignore any broadening due to finite phonon life-times or to sample mosaic. Under these conditions the intensity is simply given by integrating the resolution function over the dispersion surface, and the calculation can be further simplified by considering the dispersion surface to be planar, as a first approximation.

An expression for the intensity for the special case with $\omega_0, \mathbf{Q}_0$ on a planar dispersion surface and with no in-pile or detector collimation has been given by Collins (1963), who uses this to provide a basis for focusing considerations. We have derived in a similar way the intensity for the more general case of a planar dispersion surface passing through any point in the resolution function and including all the collimation. The resultant intensity is of the form:

$$I = I_0 \exp(-\tfrac{1}{2} H_S^2) \quad (12)$$

where I_0 is the peak intensity for $\omega_0, \mathbf{Q}_0$ lying on the dispersion plane and H_S is proportional to the distance of $\omega_0, \mathbf{Q}_0$ from the dispersion plane. The inclusion of all the collimation makes I_0 and H_S rather complex functions of the instrumental parameters; we therefore feel that the matrix notation is more convenient for calculation purposes and we have calculated in Appendix III expressions for I_0 and H_S in terms of M_{kl}.

It can be seen that if our Gaussian approximations are valid then any linear scan in $\omega, \mathbf{Q}$ space passing through the dispersion surface will be Gaussian in shape and we can readily calculate the predicted width, using computer programs to calculate M_{kl} and hence H_S. Comparing this with the observed width it should then be possible to investigate line broadening arising from finite phonon life-times. Nevertheless, in order to

choose the most favorable scans for this type of work it is still necessary to consider focusing effects.

If the sample has a finite mosaic spread we must consider the dispersion surface to have a finite width. We may consider any point on the surface to be spread out by the mosaic along the $\Delta\mathbf{Q}_y$ and $\Delta\mathbf{Q}_z$ directions and hence calculate the width from a knowledge of the mosaic spread. If the mosaic spread of the sample is Gaussian, then the width of the dispersion surface will also be Gaussian and we can readily take this effect into account in calculating the widths of experimental phonon peaks. Additional broadening due to finite phonon life-times can then be studied by comparing the calculated and observed peak widths.

Focusing effects

Focusing effects in phonon measurements are essentially of two different types. We can firstly choose our experimental parameters to optimize the peak intensity I_0 and secondly choose our mode of scanning in $\omega, \mathbf{Q}$ space to minimize the width of the observed peak. Both these types of focusing can be studied by considering the relationship of the resolution ellipsoid to the dispersion surface.

As can be seen from Figs. 4 and 5 the resolution ellipsoid is extremely aspherical and it is this property which gives rise to the focusing effects. One principal axis is always along ΔQ_z, and since we shall consider only cases for which $\mathbf{Q}_z = 0$ we shall not discuss the z dependence of the ellipsoid further. In the cases considered, which are for typical 'parallel' arrangements as illustrated in Fig. 1, one other principal axis is near the $\Delta\mathbf{Q}_x$ direction and the remaining two are rotated somewhat from $\Delta\mathbf{Q}_y$ and $\Delta\omega$. Moreover, the ellipsoid is elongated towards $\Delta\mathbf{Q}_x$ more than towards $\Delta\mathbf{Q}_y$ and is considerably elongated out of the $\Delta\omega = 0$ plane.

Since we have considered the resolution in terms of the energy lost by the neutron as a function of $\mathbf{Q}$ we can simply consider the scattering cross section as the dispersion surface $\omega(\mathbf{q})$ where $\mathbf{q}$ is a vector in $\mathbf{Q}$ space from the relevant Bragg point and the momentum of the created phonon is $-\hbar\mathbf{q}$. That is for phonon creation (energy loss) we plot $\omega(\mathbf{q})$ positive and for phonon annihilation (energy gain) we plot $\omega(\mathbf{q})$ negative.

For a planar dispersion surface intensity focusing will occur when the resolution ellipsoid and the dispersion surface are aligned to maximize the area of the surface which is enclosed by the resolution ellipsoid. For a non-planar dispersion surface we must weight each point on the surface by the resolution function at that point. For simplicity we shall consider intensity focusing to be of two types, 'Q' focusing and 'gradient' focusing.

If we consider, for purposes of illustration, a dispersion surface as some sort of cone around the Bragg point, the section of this in the $\Delta\omega = 0, \Delta Q_z = 0$ plane will be roughly circular. Since the resolution ellipsoid is elongated in this plane along ΔQ_x partial focusing will occur for particular points on the section when the sectional ellipse is aligned along the circumference as illustrated in Fig. 6.

The more important 'gradient' focusing arises when the orientation of the ellipsoid is such that the longest principal axis, which lies roughly in the $\Delta\omega, \Delta Q_y$ plane, is aligned in the dispersion surface. Since the principal ellipse lying roughly in this plane is so asymmetric marked focusing or defocusing can occur for transverse phonons with $\mathrm{grad}_{\mathbf{q}}\omega$ along Q_y, depending on the value of the gradient. Focusing effects are clearly far less for longitudinal phonons with $\mathrm{grad}_{\mathbf{q}}\omega$ along Q_x, since for

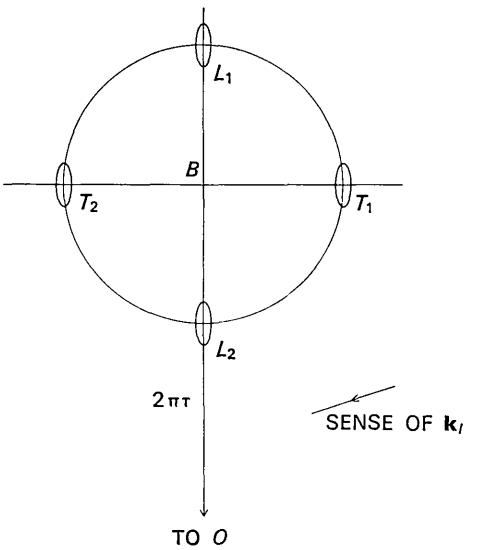

Fig. 6. Illustration of 'Q' focusing, showing the intersection of the dispersion surface and the resolution ellipsoid on the $\Delta\omega = 0$, $\Delta Q_z = 0$ plane for longitudinal (L_1, L_2) and transverse (T_1, T_2) phonons.

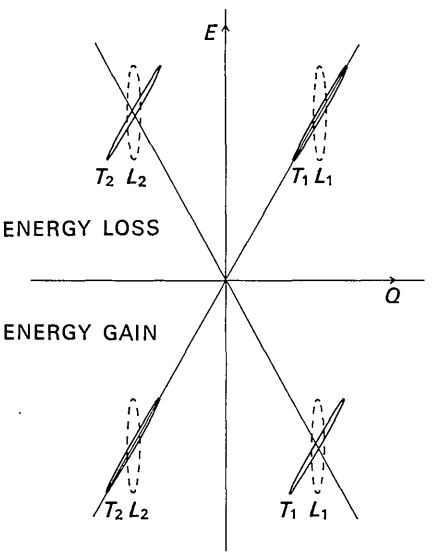

Fig. 7. Illustration of 'gradient' focusing, showing the intersection of the dispersion surface and the resolution ellipsoid on the E, Q plane for longitudinal (L_1, L_2; $\Delta\bar{Q} \parallel 2\pi\tau$) and transverse ($T_1, T_2$; $\Delta\bar{Q} \perp 2\pi\tau$) phonons.

these the ellipsoid is always tilted almost perpendicular to $\text{grad}_{\mathbf{q}}\omega$. These effects are illustrated in Fig. 7, and we may note that a focusing position for energy loss is a defocusing position for energy gain and *vice versa*. We may also note in passing that in the case of magnon scattering the gradient of the dispersion surface may be very large, resulting in better focusing being achieved for the longitudinal modes.

Figs. 6 and 7 also illustrate the conditions under which intensity focusing may be undesirable, namely when the dispersion surface has any appreciable curvature. This will occur when q is small or when the magnitude of $\text{grad}_{\mathbf{q}}\omega$ is changing rapidly, for example at Kohn anomalies, and will introduce an asymmetry into an experimental peak and give rise to a displacement of the observed maximum intensity. Although corrections can be applied if the dispersion surface is known sufficiently well, under these conditions it may well be advantageous to minimize the overlap of the resolution function and the dispersion surface in certain directions.

It is also clear from the figures that the width of a phonon peak will depend on the particular scan in $\omega, \mathbf{Q}$ space used and the ideal scan will be one normal to the dispersion surface. However, it is not always convenient to adopt a general scanning mode and it may therefore be more convenient to consider only 'constant **Q**' and 'constant ω' scans and use whichever is more suitable for a given phonon.

To achieve a more favorable focusing condition in a particular case we can select the best point in reciprocal space from those at which a particular phonon can be observed and secondly we can change our instrumental parameters, in particular d_M, d_A, and the relative senses of $2\theta_M$, $2\theta_S$ and $2\theta_A$, to give the most suitable resolution function. However, the orientation of the resolution ellipsoid is surprisingly insensitive to changes in the instrumental parameters and any focusing so achieved may be gained at the expense of over-all intensity. A series of calculations is being made to investigate these effects as fully as possible. It should be pointed out that the resolution functions for energy loss and energy gain are not equivalent owing to the difference in k_F, a factor which should also be taken into consideration.

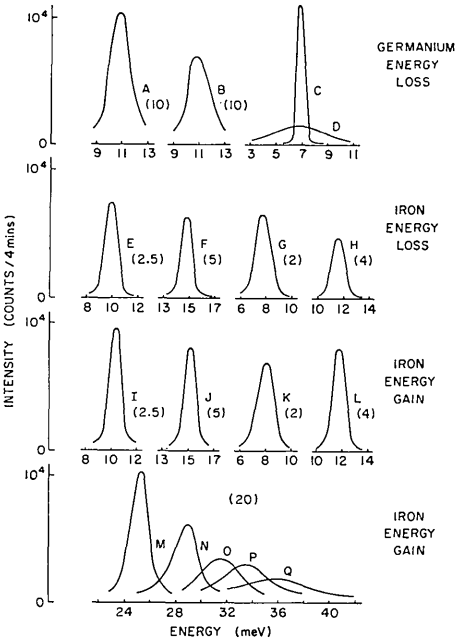

Fig. 8. Experimental 'constant Q' phonon peaks from germanium and iron. The figures in brackets are the factors by which the intensity has been multiplied.

To illustrate and support our earlier considerations we present in Fig. 8 a series of experimental phonon scans obtained by Minkiewicz and Shirane with a perfect germanium sample and an iron crystal with a mosaic spread of 7′, adopting a 'constant **Q**' mode of scan. We have deliberately included various degrees of focusing and defocusing and compared the results for energy loss and energy gain. Fig. 9 shows the points in reciprocal space at which measurements were made and in Table 1 we give the observed and predicted widths of the peaks, taking into account the mosaic spread of the sample. The theoretical resolution function used was in this case calculated from values of η_M and η_A which were measured directly and values of $\alpha_0, \alpha_1, \alpha_2, \alpha_3$ which were calculated from the dimensions of the collimators. This was compared with the observed resolution function at the germanium 200 reflection (Fig. 5) and the dimensions of the resolution ellipsoid were found to agree within a few per cent. In general the over-all agreement between the calculated and observed widths is reasonably good. However, in almost all the cases, we find the observed widths to be greater than the calculated. While it is tempting to attribute these differences to the presence of finite phonon life-times, we feel further work is called for before this point can be definitely established. Experiments on silicon at low temperatures are now in progress with a view toward checking this important feature of our results.

Table 1. *Observed and predicted widths of phonon peaks*

Phonon (see Fig. 8)	Energy (meV)	Half-width (meV) Observed	Predicted
A	10·8	1·5	1·3
B	10·8	2·0	1·8
C	6·8	0·6	0·4
D	6·8	4·2	3·4
E	9·9	1·2	1·2
F	14·8	1·0	1·2
G	7·8	1·3	1·2
H	10·5	1·2	1·1
I	10·3	1·2	0·9
J	15·2	1·0	0·8
K	8·0	1·4	1·1
L	10·7	1·1	1·0
M	25·2	1·4	1·3
N	28·8	2·0	1·7
O	31·6	3·3	2·3
P	33·5	3·8	2·9
Q	35·9	5·5	4·2

Summary

We have shown that the theoretical resolution function for Gaussian mosaic and collimation functions is such that the loci of constant probability are ellipsoids. Quite good agreement has been obtained between an observed resolution at a Bragg reflection and that calculated from the parameters of the instruments. These instrumental parameters also lead to reasonable predictions for the widths of certain phonon peaks, although there seems to be a systematic disagreement between calculated and observed widths of the phonon peaks.

The applications of these resolution ellipsoids in choosing the particular spectrometer arrangement for scanning an inelastic neutron group are obvious, both from the viewpoint of maximizing peak intensity and also with respect to establishing on an absolute basis quantitative peak widths at various points on the dispersion surface. Although we have not emphasized the point one can use this analysis to establish the conditions under which distorted peaks are to be expected or how most effectively to make scans in the immediate vicinity of Bragg peaks. Admittedly, the algebra involving the dependence of the orientation and size of the resolution ellipsoid on the spectrometer parameters is cumbersome; however, it is relatively easy to program the entire operation to provide information of value to the experimentalist.

We wish to acknowledge the numerous and detailed conversations with our colleagues, Drs Shirane, Minkiewicz, Alperin, and Pickart. In particular we are grateful to Dr G. Caglioti for his careful criticism of the manuscript and to Miss E. Wolfson for the computer programming associated with the work.

APPENDIX I
In-pile collimation

The probability function for an in-pile collimator will be:

$$P(\gamma_0,\delta_0)=\exp\left\{-\frac{1}{2}\left(\frac{\gamma_0^2}{\alpha_0^2}+\frac{\delta_0^2}{\beta_0^2}\right)\right\}, \tag{13}$$

and in addition there will be a term in $\delta_1-\delta_0$ arising from the vertical mosaic of the monochromator crystal:

$$P(\delta_1-\delta_0)=\exp\left\{-\frac{1}{2}k_I^2\left(\frac{\delta_1-\delta_0}{Q_M\eta'_M}\right)^2\right\}, \tag{14}$$

where $\mathbf{Q}_M$ is the scattering vector for the Bragg reflection of the monochromator, η'_M defines the mosaic spread in the vertical plane containing $\mathbf{Q}_M$ and we assume Δk_i to be small compared with k_I.

The horizontal in-pile divergence angle is related to the corresponding divergence angle for the monochromated beam and the Bragg angle of the monochromator.

We have that

$$k_i \sin\theta'_M = k_I \sin\theta_M , \tag{15}$$

where θ'_M is the Bragg angle of the monochromator for wave number k_i.

Therefore

$$\Delta k_i = \frac{k_I(\sin\theta_M-\sin\theta'_M)}{\sin\theta'_M} . \tag{16}$$

If we put

$$\theta'_M=\theta_M+\varepsilon \tag{17}$$

then for small ε

$$\frac{\Delta k_i}{k_I} = -\frac{\varepsilon}{\tan\theta_M} . \tag{18}$$

Now

$$2\varepsilon=\gamma_1-\gamma_0 , \tag{19}$$

so that

$$\frac{\Delta k_i}{k_I} = \frac{\gamma_0-\gamma_1}{2\tan\theta_M} \tag{20}$$

and

$$\gamma_0=2(\Delta k_i/k_I)\tan\theta_M+\gamma_1 . \tag{21}$$

For a given value of δ_1 we can integrate the vertical terms over δ_0:

$$P_{\delta_1}=\int\exp\left\{-\frac{1}{2}\left[\frac{\delta_0^2}{\beta_0^2}+k_I^2\left(\frac{\delta_1-\delta_0}{Q_M\eta'_M}\right)^2\right]\right\}d\delta_0 \tag{22}$$

$$=P_0\exp\left\{-\frac{1}{2}\left(\frac{\delta_1^2}{4\tan^2\theta_M\eta'^2_M+\beta_0^2}\right)\right\}, \tag{23}$$

where

$$P_0=\left[\frac{2\pi}{\frac{1}{\beta_0^2}+\frac{1}{4\tan^2\theta_M\eta'^2_M}}\right]^{\frac{1}{2}} . \tag{24}$$

It may be noted that for β_0 large $P_{\delta_1}\to P_0$ and the exponent becomes independent of the vertical mosaic spread.

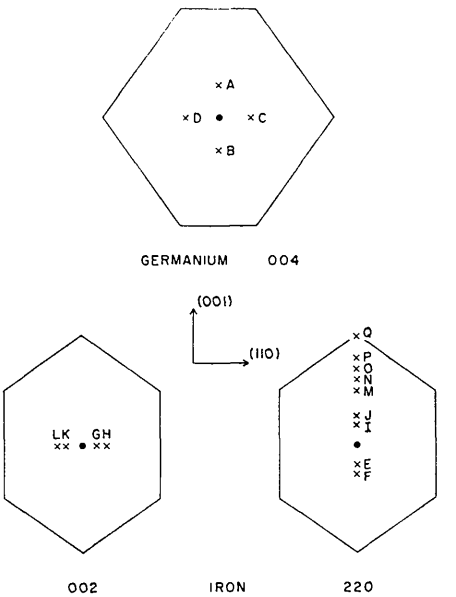

Fig. 9. The points in reciprocal space at which the peaks in Fig. 8 were measured. The Brillouin zone around each Bragg reciprocal lattice point is shown.

APPENDIX II
Derivation of the resolution matrix

For one phonon neutron scattering processes the conservation of momentum and energy are represented by the following equations:

$$\mathbf{k}_f=\mathbf{k}_i-(2\pi\tau+\mathbf{q}') \tag{25}$$

$$\frac{\hbar^2}{2m}k_f^2=\frac{\hbar^2}{2m}k_i^2-\hbar\omega \tag{26}$$

where $\mathbf{k}_i$ and $\mathbf{k}_f$ are the wave vectors of the incident and scattered neutron respectively, m is the mass of the neutron, $2\pi\tau$ is a reciprocal lattice vector and $\mathbf{q}'$ and ω are the wave vector and angular frequency of the created phonon.

The conservation of momentum [equation (25)] is illustrated in Fig. 3, where we show the most probable wave vectors, $\mathbf{k}_I$ and $\mathbf{k}_F$, for incident and scattered neutrons and define three sets of axes with respect to the vectors $\mathbf{k}_I$, $\mathbf{k}_F$ and $\mathbf{Q}(=\mathbf{k}_F-\mathbf{k}_I)$. It is convenient to define $\mathbf{q}(=-\mathbf{q}')$ as the displacement of Q from the Bragg reciprocal lattice point concerned. (See *Application to phonon measurements.*) The notation used is summarized in Table 2.

Table 2. *Notation*

$\mathbf{k}_i$	Any incident wave vector
$\mathbf{k}_f$	Any scattered wave vector
$\mathbf{k}_I$	The most probable $\mathbf{k}_i$
$\mathbf{k}_F$	The most probable $\mathbf{k}_f$
$\Delta\mathbf{k}_i$	$\mathbf{k}_i-\mathbf{k}_I$
$\Delta\mathbf{k}_f$	$\mathbf{k}_f-\mathbf{k}_F$
α_j	Horizontal collimation angle
β_j	Vertical collimation angle
γ_j	Horizontal divergence angle
δ_j	Vertical divergence angle
$j=0$	In-pile region
$j=1$	Monochromator to sample
$j=2$	Sample to analyzer
$j=3$	Analyzer to detector
η_M	Horizontal mosaic spread of monochromator
η_A	Horizontal mosaic spread of analyzer

If we put $\Delta\mathbf{k}_i=\mathbf{k}_i-\mathbf{k}_I$ and $\Delta\mathbf{k}_f=\mathbf{k}_f-\mathbf{k}_F$ then the change in $\mathbf{Q}$ from the most probable value is given from equation (25) as

$$\Delta\mathbf{Q}=\Delta\mathbf{k}_f-\Delta\mathbf{k}_i\,. \tag{27}$$

If $\Delta\mathbf{k}_i$ has components x_1,y_1,z_1 along the axes i_1,j_1,l_1 defined with respect to $\mathbf{k}_I$ and $\Delta\mathbf{k}_f$ has components x_2,y_2,z_2 along axes i_2,j_2,l_2 defined with respect to $\mathbf{k}_F$, then we can readily determine their components along axes i_0,j_0,l_0 defined with respect to $\mathbf{Q}$.

We then have

$$\Delta\mathbf{k}_i=(x_1b+y_1a)\mathbf{i}_0+(-x_1a+y_1b)\mathbf{j}_0+z_1\mathbf{l}_0 \tag{28a}$$

$$\Delta\mathbf{k}_f=(x_2B+y_2A)\mathbf{i}_0+(-x_2A+y_2B)\mathbf{j}_0+z_2\mathbf{l}_0\,, \tag{28b}$$

where

$$a=\sin\Phi\quad A=\sin(2\theta_S+\Phi)$$
$$b=\cos\Phi\quad B=\cos(2\theta_S+\Phi)\,, \tag{29}$$

Φ being the angle between $\mathbf{k}_I$ and $-\mathbf{Q}$.

From equation (27) we then have

$$\Delta Q_x=x_2B+y_2A-x_1b-y_1a \tag{30a}$$

$$\Delta Q_y=-x_2A+y_2B+x_1a-y_1b \tag{30b}$$

$$\Delta Q_z=z_2-z_1\,. \tag{30c}$$

From equation (26) we have also

$$\frac{\hbar}{m}x_2k_F=\frac{\hbar}{m}x_1k_I-\Delta\omega \tag{31a}$$

$$x_2=\frac{x_1k_I-\Delta\Omega/2}{k_F} \tag{31b}$$

$$=\lambda x_1-\Delta\Omega/(2k_F)\,, \tag{31c}$$

where

$$\Omega=\frac{2m}{\hbar}\omega \tag{32a}$$

and

$$\lambda=k_I/k_F\,. \tag{32b}$$

Eliminating y_2 and y_1 from equations (30a) and (30b) respectively we obtain

$$y_1\alpha=B\Delta Q_x-A\Delta Q_y+x_1\beta-x_2 \tag{33a}$$

$$y_2\alpha=b\Delta Q_x-a\Delta Q_y+x_1-x_2\beta\,, \tag{33b}$$

where

$$\alpha=\sin 2\theta_S\quad \beta=\cos 2\theta_S\,. \tag{34}$$

Substituting for x_2 from equation (31) we have

$$y_1=[B\Delta Q_x-A\Delta Q_y-x_1(\lambda-\beta)+\Delta\Omega/(2k_F)]/\alpha \tag{35a}$$

$$y_2=[b\Delta Q_x-a\Delta Q_y-x_1(\beta\lambda-1)+\beta\Delta\Omega/(2k_F)]/\alpha\,. \tag{35b}$$

If we write

$$y_1=Cx_1+D \tag{36a}$$

$$y_2=Ex_1+F \tag{36b}$$

$$x_2=\lambda x_1+H \tag{36c}$$

and put

$$\Delta Q_x=X_1,\Delta Q_y=X_2,\Delta\omega=X_4 \tag{37}$$

then we have

$$D=d_1X_1+d_2X_2+d_4X_4 \tag{38a}$$

$$F=f_1X_1+f_2X_2+f_4X_4 \tag{38b}$$

$$H=h_1X_1+h_2X_2+h_4X_4\,, \tag{38c}$$

where the values of d_j, f_j and h_j are given from equations (32), (35) and (36) as:

$$\begin{array}{lll} d_1=B/\alpha & d_2=-A/\alpha & d_4=m/(\alpha\hbar k_F) \\ f_1=b/\alpha & f_2=-a/\alpha & f_4=\beta m/(\alpha\hbar k_F) \\ h_1=0 & h_2=0 & h_4=-m/(\hbar k_F) \end{array} \tag{39}$$

and

$$C=-(\lambda-\beta)/\alpha \tag{40a}$$

$$E=-(\beta\lambda-1)/\alpha\,. \tag{40b}$$

The resolution function, ignoring the effect of vertical collimation, is given by

$$R_H\propto\int_{-\infty}^{\infty}\exp\{-\tfrac{1}{2}[(a_1x_1+a_2y_1)^2+a_3^2y_1^2+a_4^2y_2^2 +(a_5x_2+a_6y_2)^2 +(a_7x_1+a_8y_1)^2+(a_9x_2+a_{10}y_2)^2]\}dx_1dy_1dx_2dy_2\,, \tag{41}$$

where a_j is given in terms of the collimation parameters:

$$a_1=\frac{\tan\theta_M}{\eta_M k_I} \quad a_4=\frac{1}{\alpha_2 k_F} \quad a_7=\frac{2\tan\theta_M}{\alpha_0 k_I}$$
$$a_2=\frac{1}{\eta_M k_I} \quad a_5=\frac{\tan\theta_A}{\eta_A k_F} \quad a_8=\frac{1}{\alpha_0 k_I}$$
$$a_3=\frac{1}{\alpha_1 k_I} \quad a_6=\frac{-1}{\eta_A k_F} \quad a_9=\frac{2\tan\theta_A}{\alpha_3 k_F}$$
$$a_{10}=-\frac{1}{\alpha_3 k_F} \qquad (42)$$

[See equations (6), (7) and (8)].

We are assuming that Δk_i and Δk_f are small compared with k_I and k_F and that the usual small angle approximations are valid, so that $y_1=k_I\gamma_1$, *etc.* We may note that in general the resolution function is an integral over four variables but that for elastic scattering $dx_1=dx_2$ and the number of variables is reduced to three.

Writing equation (41) as

$$R_H\propto\int_{-\infty}^{\infty}\exp\{-\tfrac{1}{2}[A'x_1^2+B'x_1+C']\}dx_1 \qquad (43)$$

and putting

$$b_0=a_1a_2+a_7a_8$$
$$b_1=a_2^2+a_3^2+a_8^2$$
$$b_2=a_4^2+a_6^2+a_{10}^2$$
$$b_3=a_5^2+a_9^2$$
$$b_4=a_5a_6+a_9a_{10}$$
$$b_5=a_1^2+a_7^2 \qquad (44)$$

we have

$$A'=2b_0C+b_1C^2+b_2E^2+b_3\lambda^2+2b_4\lambda E+b_5 \qquad (45a)$$
$$B'=2[(b_0+b_1C)D+(b_2E+b_4\lambda)F+(b_3\lambda+b_4E)H] \qquad (45b)$$
$$C'=b_1D^2+b_2F^2+b_3H^2+2b_4FH\,, \qquad (45c)$$

and on integration equation (43) becomes

$$R_H=R_0^H\exp\left\{-\frac{1}{2}\left(C'-\frac{B'^2}{4A'}\right)\right\}. \qquad (46)$$

Hence the equation

$$C'-\frac{B'^2}{4A'}=P \qquad (47)$$

will represent the locus of points of probability $R_0^H\exp(-p/2)$.

From equations (45) it can be shown that

$$C'-\frac{B'^2}{4A'}=g_0D^2+g_1F^2+g_2H^2+g_3FH+g_4DF+g_5DH\,, \qquad (48)$$

where

$$g_0=b_1-(b_0+b_1C)^2/A'$$
$$g_1=b_2-(b_2E+b_4\lambda)^2/A'$$
$$g_2=b_3-(b_3\lambda+b_4E)^2/A'$$
$$g_3=2b_4-2(b_2E+b_4\lambda)(b_3\lambda+b_4E)/A'$$
$$g_4=-2(b_0+b_1C)(b_2E+b_4\lambda)/A'$$
$$g_5=-2(b_0+b_1C)(b_3\lambda+b_4E)/A'\,. \qquad (49)$$

Hence from equation (38) we see that equation (47) represents an ellipsoid in $\Delta Q_x,\Delta Q_y,\Delta\omega$ space and writing this as

$$\sum_{k,l=1,2,4}\sum M_{kl}X_kX_l=p \qquad (50)$$

we have that

$$M_{kl}=\tfrac{1}{2}[2g_0d_kd_l+2g_1f_kf_l+2g_2h_kh_l+g_3(f_kh_l+f_lh_k)+g_4(d_kf_l+d_lf_k)+g_5(d_kh_l+d_lh_k)] \qquad (51)$$

for k and $l=1$, 2 or 4.

Since the vertical term in the resolution function is independent of the horizontal term we have

$$M_{k3}=M_{3l}=0 \qquad (52)$$
for $k,l\neq 3$
and $X_3=\Delta Q_z$. $\qquad (53)$

The vertical term is given by

$$R_V\propto\int_{-\infty}^{\infty}\exp\{-\tfrac{1}{2}[a_{11}^2+a_{12}^2z_2^2]\}dz_1dz_2\,, \qquad (54)$$

where

$$a_{11}^2=\frac{1}{(4\tan^2\theta_M\eta_M'^2+\beta_0^2)k_I^2}+\frac{1}{\beta_1^2k_I^2} \qquad (55a)$$

$$a_{12}^2=\frac{1}{\beta_2^2k_F^2}+\frac{1}{(4\tan^2\theta_A\eta_A'^2+\beta_3^2)k_F^2}\,. \qquad (55b)$$

We have

$$X_3=\Delta Q_z=z_2-z_1\,. \qquad (56)$$

Substituting this into equation (54) we obtain

$$R_V\propto\exp\{-\tfrac{1}{2}M_{33}X_3^2\}\,,$$

where

$$M_{33}=-\frac{a_{11}^2a_{12}^2}{a_{11}^2+a_{12}^2}\,. \qquad (57)$$

Hence the complete resolution function is

$$R=R_0\exp\{-\tfrac{1}{2}\sum_{k=1,l=1}^{4}\sum^{4}M_{kl}X_kX_l\} \qquad (58)$$

and the probability ellipsoid in $\Delta\omega,\Delta\mathbf{Q}$ space is:

$$\sum_{k=1,l=1}^{4}\sum^{4}M_{kl}X_kX_l=p\,, \qquad (59)$$

where M_{kl} is defined by equations (51), (52) and (57).

APPENDIX III
Width of phonon peak

If we take our origin for $\Delta\omega_0,\Delta\mathbf{Q}_0$ to be the point of intersection of the scan with the dispersion plane we can define the scan by the relation

$$\Delta\omega_0=\mathbf{s}\,.\,\Delta\mathbf{Q}_0\,, \qquad (60)$$

$\Delta\omega_0$ and ΔQ_0 representing the displacement of the ω_0 and Q_0 from this origin, and $\mathbf{s}$ being a unit vector in the direction of the scan.

We consider a planar dispersion surface through the point $\Delta\omega_0,\Delta\mathbf{Q}_0$ (see *Application to phonon measurements*; *Focusing effects*) we can write

$$\Delta\omega = \mathrm{grad}_{\mathbf{q}}\omega \,.\, (\Delta\mathbf{Q} - \Delta\mathbf{Q}_0) + \Delta\omega_0 \qquad (61)$$

for any point on this surface, and

$$\mathbf{c} = -\mathrm{grad}_{\mathbf{q}}\omega \qquad (62)$$

is the group velocity of the phonon.

If c_1, c_2 and c_3 are the components of $\mathbf{c}$ along ΔQ_x, ΔQ_y and ΔQ_z respectively and we consider only the case of a symmetry plane such that $c_3=0$, then using the same notation as before we can write equation (61) as

$$X_4 = -c_1X_1 - c_2X_2 + W\,, \qquad (63)$$

where

$$W = \Delta\omega_0 + \mathbf{c} \,.\, \Delta\mathbf{Q}_0 = (\mathbf{s}+\mathbf{c}) \,.\, \Delta\mathbf{Q}_0 \qquad (64)$$

The observed intensity is then obtained by integrating the resolution function over the plane defined by equation (63). Substituting the relation in this equation into the exponent of the resolution function [equation (59)] we have:

$$\sum_{k=1}^{4}\sum_{l=1}^{4} M_{kl}X_kX_l = M_{11}X_1^2 + M_{22}X_2^2 + M_{33}X_3^2 + M_{44}(-c_1X_1 - c_2X_2 + W)^2 + 2M_{12}X_1X_2 + 2(M_{14}X_1 + M_{24}X_2)(-c_1X_1 - c_2X_2 + W) \qquad (65)$$

and on integration over X_1,X_2 and X_3 we obtain

$$I_W = 2\pi R_{33}G_1G_2 \exp\{-\tfrac{1}{2}G_3^2W^2\}\,, \qquad (66)$$

where

$$R_{33} = \int_{-\infty}^{\infty} \exp\{-\tfrac{1}{2}M_{33}X_3^2\}dX_3 \qquad (67a)$$

$$G_1 = 1/(M_{11} + c_1^2M_{44} - 2c_1M_{14} \qquad (67b)$$

$$G_2 = 1/[M_{22} + c_2^2M_{44} - 2c_2M_{24} - G_1\{M_{12} - c_1M_{24} - c_2(M_{14} - c_1M_{44})\}^2] \qquad (67c)$$

$$G_3^2 = M_{44} + G_1c_1(M_{14} - c_1M_{44})^2 - G_2[-c_2M_{44} + M_{24} - G_1(M_{14} - c_1M_{44}) \{M_{12} - c_1M_{24} - c_2(M_{14} - c_1M_{44})\}]^2\,. \qquad (67d)$$

Comparing equation (66) with equation (12) we see that the peak intensity is simply

$$I_0 = 2\pi R_{33}G_1G_2 \qquad (68)$$

and

$$H_S = G_3W\,. \qquad (69)$$

The characteristic width of a linear scan in $\Delta\omega$,$\Delta\mathbf{Q}$ space in terms of W is thus $1/G_3$.

We note that in this derivation we have assumed that over the range of the scan, *i.e.* the range of $\Delta\omega_0$ and $\Delta\mathbf{Q}_0$ values, that the resolution function itself does not change [see equation (11)]. This is valid only if the range of $\Delta\omega_0$ and $\Delta\mathbf{Q}_0$ is small compared with ω_0 and $\mathbf{Q}_0$, the positions corresponding to the intensity maximum in the scan.

References

BARRETT, C. S., MUELLER, M. H. & HEATON, L. (1963). *Rev. Sci. Instrum.* **34**, 347.

CAGLIOTI, G. (1964). *Acta Cryst.* **17**, 1202.

CAGLIOTI, G., PAOLETTI, A. & RICCI, F. P. (1958). *Nucl. Instr. Methods*, **3**, 223.

CAGLIOTI, G., PAOLETTI, A. & RICCI, F. P. (1960). *Nucl. Instr. Methods*, **9**, 195.

CAGLIOTI, G. & RICCI, F. P. (1962). *Nucl. Instr. Methods*, **15**, 155.

CAGLIOTI, G. & TOCCHETTI, D. (1964). I.A.E.A. International Symposium on the Inelastic Scattering of Neutrons, Bombay.

CAGLIOTI, G. & TOCCHETTI, D. (1965). *Nucl. Instr. Methods*, **32**, 181.

COLLINS, M. F. (1963). *Brit. J. Appl. Phys.* **14**, 805.

SAILOR, V. L., FOOTE, H. L., JR., LANDON, H. H. & WOOD, R. E. (1956). *Rev. Sci. Instrum.* **27**, 26.

SHULL, C. G. (1960). M.I.T. Technical Report AFOSR-TR-60-111.

WILLIS, B. T. M. (1960). *Acta Cryst.* **13**, 763.

Acta Cryst. (1967). **23**, 367

Application de la Méthode d'Addition Symbolique: Structure Cristalline de l'Acide *N*-α-Naphtyltetrahydro-1,2,3,6-phtalamique

PAR J. P. MORNON

Laboratoire des Rayons X, IRCHA, 12 Quai Henri IV, Paris 4e

(*Reçu le 23 février* 1967)

The symbolic addition method has been used to determine the crystal structure of *N*-α-naphthyl-1,2,3,6-tetrahydrophthalamic acid. The material crystallizes in the space group $P2_1/c$ with cell dimensions $a=17{\cdot}43$, $b=4{\cdot}97$, $c=22{\cdot}90$ Å, $\beta=132°$. A comparison on structural aspects is made with *N*-α-naphthyl-4-chlorophthalamic acid.

Introduction

La détermination des structures cristallines de plusieurs acides arylphtalamiques a été entreprise pour contribuer à l'explication de leur mode d'action sur les végétaux. En effet certains de ces composés inversent le sens du géotropisme de racines végétales (Mentzer, Molho & Pacheco, 1950). Cette résolution de structure par application de la méthode d'addition symbolique fait suite à celle de l'acide *N*-α-naphtylchloro-4-phtalamique (Mornon, 1966). L'acide *N*-α-naphtyl-tétrahydro-1,2,3,6-phtalamique a pour formule: